Acta Crystallographica Section D
Biological Crystallography
ISSN 1399-0047

Structural characterization and comparison of the large subunits of IPM isomerase and homoaconitase from *Methanococcus jannaschii*

Eun Hye Lee,‡ Kitaik Lee‡ and Kwang Yeon Hwang*

Division of Biotechnology, College of Life Sciences and Biotechnology, Korea University, Anam-dong-5, Seongbuk-gu, Seoul 136-701, Republic of Korea

‡ These authors made equal contributions.

Correspondence e-mail: chahong@korea.ac.kr

Received 3 June 2013
Accepted 13 December 2013

PDB references: ox-MJ0499, 4kp1; red-MJ0499, 4nqy; MJ1003, 4kp2

The aconitase family of proteins includes three classes of hydro-lyase enzymes: aconitases, homoaconitases and isopropylmalate (IPM) isomerases. They have a common Fe–S cluster-binding site and catalyze the isomerization of specific substrates by sequential dehydration and hydration. The archaeon *Methanococcus jannaschii* contains two aconitase family proteins, IPM isomerase and homoaconitase, which have 50% sequence identity. These two enzymes are heterodimeric proteins composed of large and small subunits encoded by separate genes. Although structures have been reported for the small subunits of the two enzymes, the first structures of oxidized and reduced forms of the large subunit of IPM isomerase (ox-MJ0499 and red-MJ0499, respectively) from *M. jannaschii* are reported here at 1.8 and 2.7 Å resolution, respectively, together with the structure of the large subunit of homoaconitase (MJ1003) at 2.5 Å resolution. The structures of both proteins have unbound Fe–S clusters and contain a fourth cysteine in the active site. The active site of MJ1003 is homologous to that of aconitase, whereas MJ0499 has significant structural distortion at the active site compared with aconitase. In addition, significant large conformational changes were observed in the active site of red-MJ0499 when compared with ox-MJ0499. The active sites of the two proteins adopt two different states before changing to the Fe–S cluster-bound 'activated' state observed in aconitase. MJ1003 has an 'open' active site, which forms an active pocket for the cluster, while ox-MJ0499 has a 'closed' active site, with four cysteines in disulfide bonds. These data will be helpful in understanding the biochemical mechanism of clustering of the Fe–S protein family.

1. Introduction

Three classes of hydro-lyase enzymes, aconitases, homoaconitases and isopropylmalate (IPM) isomerases, are classified as aconitase family proteins (Gruer *et al.*, 1997). Aconitase (EC 4.2.1.3) employs an Fe–S cluster to catalyze the stereospecific isomerization of citrate to isocitrate *via cis*-aconitate in the tricarboxylic acid cycle (Beinert & Kennedy, 1993). Homoaconitase enzymes catalyze hydro-lyase reactions in the α-aminoadipate pathway for lysine biosynthesis and in the 2-oxo-suberate pathway for methanogenic coenzyme B biosynthesis. Homoaconitase (EC 4.2.1.36; homoaconitate hydratase) only catalyzes the hydration of *cis*-homoaconitate to form homoisocitrate (Strassman & Ceci, 1966), whereas methanogen homoaconitase (EC 4.2.1.114) catalyzes the

complete isomerization of homocitrate to homoisocitrate (Drevland *et al.*, 2008). IPM isomerase (EC 4.2.1.33) catalyzes the reversible dehydration of 2-IPM to 2-isopropylmaleate and the subsequent addition of water, yielding 3-IPM, in the leucine-biosynthesis pathway (Cole *et al.*, 1973; Gross *et al.*, 1963). All three classes of enzyme catalyze the isomerization of α-hydroxy acids to β-hydroxy acids by sequential dehydration and hydration (Beinert *et al.*, 1996).

The archaeon *Methanococcus jannaschii* is a hyperthermophilic methanogen that produces energy through methanogenesis (Bult *et al.*, 1996; Reeve, 1992). This organism uses three different 2-oxoacid elongation pathways that extend the chain length of precursors in leucine, isoleucine and coenzyme B biosynthesis (Drevland *et al.*, 2007). Each 2-oxoacid elongation pathway consists of three reaction steps. The first is the transfer of an acetyl group from acetyl-coenzyme A (CoA) to the 2-oxoacid, the second reaction is catalyzed by a hydrolyase enzyme and the last reaction is NAD^+-dependent oxidation and decarboxylation to form a new 2-oxoacid (Howell *et al.*, 1998; Drevland *et al.*, 2008; White, 1989). This organism utilizes two enzymes, homoaconitase and IPM isomerase, to catalyze the second isomerization in these 2-oxoacid elongation pathways. Homoaconitase catalyzes the second isomerization in coenzyme B biosynthesis and has broad specificity for *cis*-unsaturated tricarboxylic acids (Drevland *et al.*, 2008). IPM isomerase catalyzes the second isomerization in both leucine and isoleucine biosynthesis. This enzyme has a dual function as a citramalate isomerase, which catalyzes the isomerization of (*R*)-citramalate to β-methylmalate in isoleucine biosynthesis (Howell *et al.*, 1999).

Two aconitase family enzymes, IPM isomerase and homoaconitase, are present in all prokaryotic and several eukaryotic species. Based on their subunit structures, these proteins are divided into monomeric fungal, heterodimeric eubacterial and archaeal enzymes (Fultz & Kemper, 1981). *M. jannaschii* has two pairs of genes that correspond to the large (~48 kDa) and small (~18 kDa) subunits of the two enzymes, which share 50% identity (Bult *et al.*, 1996). The *leuC* and *leuD* genes encode the large (MJ0499) and small (MJ1277) subunits of IPM isomerase, respectively, and the *hacA* and *hacB* genes encode the large (MJ1003) and small (MJ1271) subunits of homoaconitase, respectively. These two enzymes are homologous to aconitase, which is composed of a single polypeptide with four domains (Hentze & Argos, 1991). The large subunit is homologous to domains 1–3, which contain the cluster-binding site, and the small subunit is homologous to domain 4, which is responsible for substrate specificity (Yasutake *et al.*, 2004). The substrates of aconitase family enzymes share a common backbone structure, but have a different γ-moiety that is recognized by the small subunit (Manikandan *et al.*, 2011; Jeyakanthan *et al.*, 2010).

Aconitase has been extensively studied for decades, and structures have been solved with various substrates and ligands. In contrast, only structures of the small subunits of other aconitase family enzymes have been reported (Lauble *et al.*, 1992; Robbins & Stout, 1989). The small-subunit structure studies found that the variable loop region is important for substrate recognition (Jeyakanthan *et al.*, 2010; Lee *et al.*, 2012). Based on their similarity to aconitase, IPM isomerases and homoaconitases are predicted to have a conserved Fe–S cluster-binding site that consists of three cysteine ligands and several substrate-binding residues (Lloyd *et al.*, 1999). We have solved the large-subunit structures of *M. jannaschii* IPM isomerase and homoaconitase. These methanogen proteins have no Fe–S cluster at the active site and show several other differences compared with aconitase. This information provides a persuasive explanation for the structural differences observed between aconitase family proteins and the mechanism of clustering of the Fe–S protein family.

2. Materials and methods

2.1. Cloning, expression and purification

Genes encoding the large subunits of IPM isomerase and homoaconitase, *leuC* (MJ0499) and *hacA* (MJ1003), respectively, were amplified from *M. jannaschii* chromosomal DNA. The amplified gene fragments were cloned into the pET-28a expression vector, which includes an N-terminal hexahistidine tag. The resulting constructs were transformed into *Escherichia coli* BL21(DE3) Star cells. The recombinant proteins were overexpressed and purified as follows. Cells were grown in LB medium with 50 μg ml^{-1} kanamycin at 37°C to an optical density at 600 nm (OD_{600}) of ~0.6 and protein expression was then induced by the addition of 0.3 m*M* IPTG. Cells were grown overnight at 18°C and harvested by centrifugation, and the cell pellet was resuspended in ice-cold lysis buffer (20 m*M* Tris–HCl pH 7.5, 500 m*M* NaCl, 4 m*M* $MgCl_2$, 5 m*M* imidazole). The cells were lysed by sonication and centrifuged, and the supernatant containing amplified protein was applied onto a HisTrap HP column (GE Healthcare) equilibrated with lysis buffer. The recombinant protein was eluted with an imidazole gradient (to 500 m*M*) and then applied onto a size-exclusion chromatography column (Superdex 200) in buffer consisting of 10 m*M* Tris–HCl pH 8.0, 100 m*M* NaCl. The purified proteins were >95% pure by SDS–PAGE analysis and were concentrated to 10 mg ml^{-1} for crystallization. For phase determination, selenomethionine-substituted MJ0499 was prepared using the same method as used for the native protein. Red-MJ0499 was prepared by addition of 1 m*M* TCEP–HCl [tris(2-carboxyethyl)phosphine hydrochloride] to the elution buffer.

2.2. Crystallization and data collection

Initial crystallization experiments on ox-MJ0499 and MJ1003 were performed by the sitting-drop vapour-diffusion method. Crystals suitable for data collection were obtained *via* hanging-drop vapour diffusion at 20°C by mixing 1.5 µl protein solution and 1.5 µl precipitant solution. Crystals of ox-MJ0499 were obtained from a reservoir solution consisting of 60% 2-methyl-2,4-pentanediol (MPD), 0.1 *M* Bicine pH 9.7. The crystal was directly flash-cooled from the crystallization drop in liquid nitrogen and subjected to X-ray diffraction. Single-wavelength anomalous dispersion data for the SeMet-

Table 1
Data-collection and refinement statistics.

Each data set was collected from a single crystal. Values in parentheses are for the highest resolution shell.

	Ox-MJ0499 (PDB entry 4kp1)	Red-MJ0499 (PDB entry 4nqy)	MJ1003 (PDB entry 4kp2)
Diffraction data			
Space group	*I*222	$P4_1$	$P2_12_12_1$
Asymmetric unit	Monomer	Dimer	Dimer
Unit-cell parameters (Å)	*a* = 77.4, *b* = 98.8, *c* = 142.6	*a* = 117.0, *b* = 117.0, *c* = 84.9	*a* = 68.3, *b* = 103.1, *c* = 112.9
Resolution (Å)	1.80 (1.85–1.80)	2.60 (2.74–2.60)	2.50 (2.54–2.50)
Total reflections	382216	465340	124785
Unique reflections	62569	35369	27050
$\langle I/\sigma(I)\rangle$	19.6 (2.2)	15.7 (2.3)	10.7 (1.8)
Completeness (%)	96.9 (95.7)	99.8 (99.8)	96.1 (91.8)
R_{merge}	0.075 (0.451)	0.096 (1.194)	0.099 (0.314)
Multiplicity	5.5 (3.7)	13.2 (12.2)	5.0 (3.1)
Wilson *B* factor (Å^2)	25.4	68.1	37.6
Refinement			
R_{cryst} (%)	21.4	20.4	22.6
R_{free} (%)	25.2	24.5	27.7
Protein atoms	3221	6239	6418
Ligand atoms	42	1	0
Solvent atoms	212	21	52
Average *B* (Å^2)	35.027	92.703	54.962
R.m.s. deviations			
Bond lengths (Å)	0.012	0.006	0.002
Angles (°)	1.384	1.277	0.563
Ramachandran plot			
Most favoured (%)	97.4	96.3	93.8
Allowed (%)	2.6	3.5	5.7
Disallowed (%)	0	0.2	0.5

substituted crystal were collected at a wavelength of 0.9795 Å on beamline 4A at the Pohang Light Source (Pohang, Republic of Korea) to a maximum resolution of better than 1.8 Å and were processed using the *HKL*-2000 package (Otwinowski & Minor, 1997). The crystal belonged to the orthorhombic space group *I*222, with unit-cell parameters *a* = 77.4, *b* = 93.8, *c* = 142.6 Å, and the asymmetric unit contained one molecule. The red-MJ0499 crystal was obtained using 20% PEG 400, 0.1 *M* Tris pH 8.2, 0.5% LDAO (*n*-dodecyl-*N*,*N*-dimethylamine-*N*-oxide). The crystal was soaked in 25% glycerol for a few seconds and X-ray diffraction were collected on the 5C beamline at PLS (Pohang, Repbulic of Korea) to a maximum resolution of better than 2.6 Å. The X-ray data were indexed, integrated by *iMosflm* (Battye *et al.*, 2011) and scaled by *SCALA* (Evans, 2006) from the *CCP*4 software package (Winn *et al.*, 2011). The crystal belonged to space group $P4_1$, with unit-cell parameters *a* = *b* = 117.0, *c* = 84.9 Å, and the asymmetric unit contained two molecules. Crystals of MJ1003 were obtained from 18% Jeffamine ED-2001 pH 7.0, 0.1 *M* sodium citrate pH 5.5. For data collection, the crystal was soaked in 50% Jeffamine ED-2001 pH 7.0 for a few seconds and flash-cooled in liquid nitrogen. Diffraction data were collected on the BL26B1 beamline of Spring-8 (Osaka, Japan) at a wavelength of 1.0000 Å to a maximum resolution of better than 2.5 Å. The X-ray data were processed using the *HKL*-2000 package (Otwinowski & Minor, 1997). The crystal belonged to the orthorhombic space group $P2_12_12_1$, with unit-cell parameters *a* = 68.3, *b* = 103.1, *c* = 112.9 Å, and the asymmetric unit contained two molecules.

2.3. Structure determination

The initial phase of MJ0499 was obtained and improved by *autoSHARP* (Vonrhein *et al.*, 2007), resulting in 60% of the modelled residues being automatically built. Further model building was performed using *Coot* (Emsley & Cowtan, 2004), and iterative cycles of refinement were performed with *PHENIX* (Adams *et al.*, 2010). The final model was validated using *MolProbity* (Chen *et al.*, 2010) and had R_{cryst} = 21.4% and R_{free} = 25.2%. The MJ1003 and red-MJ0499 structures were determined by molecular replacement using the ox-MJ0499 structure as a search model with the *Phaser* program in *PHENIX* (Adams *et al.*, 2010). Further model building was performed using *Coot* (Emsley & Cowtan, 2004) and refinement was performed with *REFMAC*5 (Murshudov *et al.*, 2011) in *CCP*4 (Winn *et al.*, 2011) and *PHENIX*. The final models of the two structures were validated using *MolProbity* and had R_{cryst} = 20.4% and R_{free} = 24.5% for red-MJ0499 and R_{cryst} = 22.6% and R_{free} = 27.7% for MJ1003. A summary of the statistics of data collection and structure refinement is provided in Table 1.

3. Results

3.1. Overall structure of MJ0499

The 1.8 Å resolution crystal structure of ox-MJ0499 was determined by SAD and one molecule was contained in the asymmetric unit. One molecule was refined with 423 residues (residues 2–424), lacking the N-terminal fusion tag and the starting methionine residue. The monomer consisted of 18 α-helices and 17 β-strands, which assembled into a triangle-shaped three-domain structure (Fig. 1*a*). The structure is composed of a three-layer $\alpha/\beta/\alpha$ sandwich (domain 1; residues 1–157), a two-layer α/β sandwich (domain 2; residues 158–273) and domain 3 (residues 274–424). The three domains are tightly associated around the active site, where two disulfide bonds (Cys102–Cys365 and Cys304–Cys368) are formed. We found that four molecules of MPD and one molecule of DMPD (2,4-dimethylpentane-2,4-diol) were bound in MJ0499. They originated from the crystallization solution, which contained 60% MPD. Three MPD molecules are bound at the solvent-exposed surfaces of domains 1 and 2, and one MPD molecule and the DMPD molecule are bound in a cavity of domain 3.

Ox-MJ0499 was purified as two separate forms in solution: as a monomer (from the approximate molecular weight according to gel filtration) and as a dimer. Crystals of the monomer form were successfully grown and were used to determine the crystal structure. Several molecular contacts were observed at the interface between symmetrically oriented molecules in the crystal. At the edge of domain 1, residues 71–73 were closely associated with a neighbouring monomer at the crystallographic position of *I*222 $(-x-1, y, -z)$

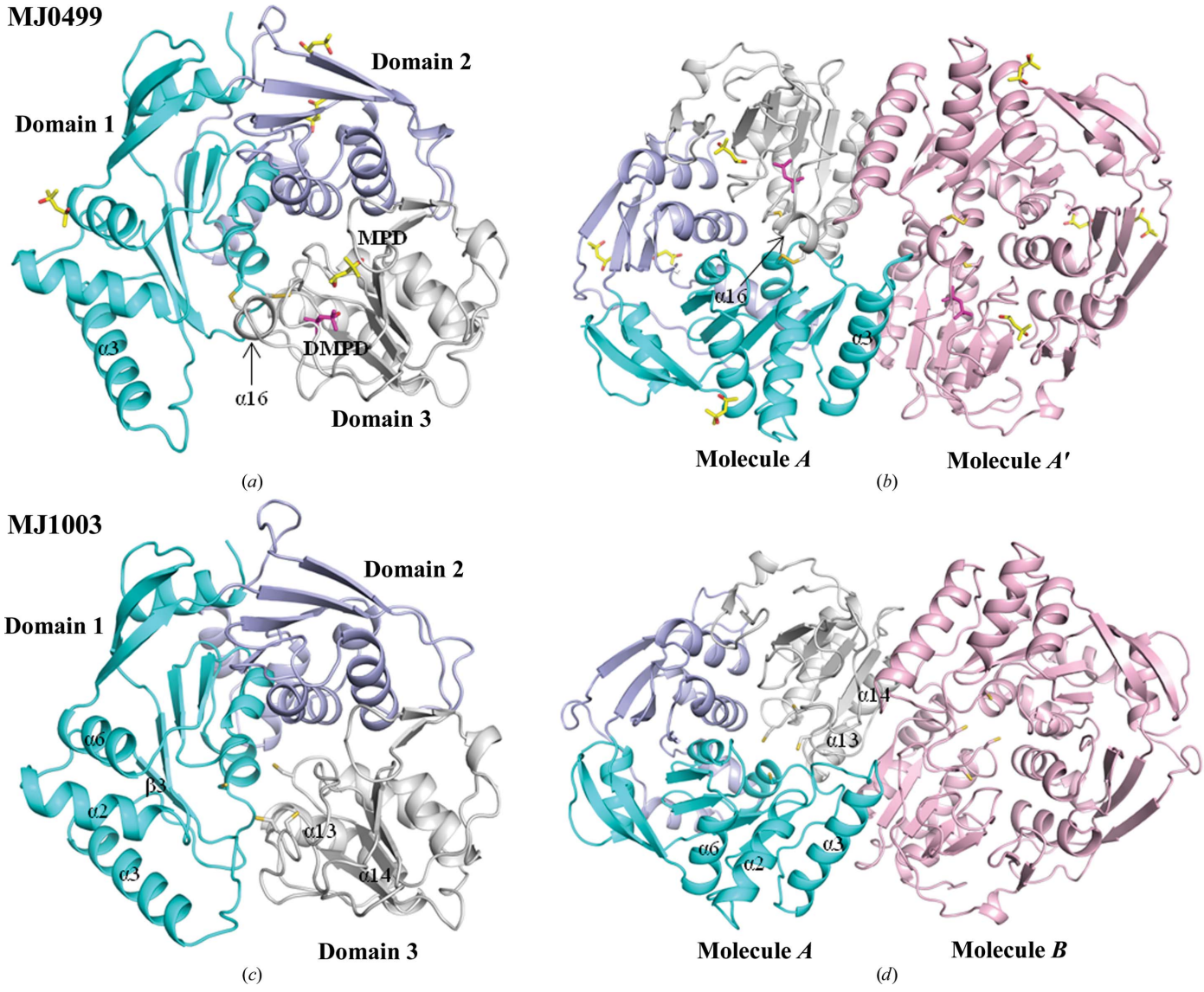

Figure 1
(*a*) Overall structure of MJ0499. The monomer consists of three domains (domain 1, cyan; domain 2, light blue; domain 3, grey). The bound molecules, four MPD (yellow) and one DMPD (magenta), are represented by stick models. (*b*) The MJ0499 crystal dimerizes with a symmetrical molecule (light pink), and the α3 and α16 helices contribute to dimer interaction. (*c*) Overall structure of MJ1003. The monomer consists of three domains (same colour representation as MJ0499). (*d*) The MJ1003 dimer crystal structure with molecule *B* (light pink). The α3 helix contributes to the dimer interface. MPD, 2-methylpentane-2,4-diol; DMPD, 2,4-dimethylpentane-2,4-diol.

symmetry. Residues Asp71 and Ile73′ (where a prime indicates a residue from the other monomer) make close contact and show continuous electron density (Supplementary Fig. S1[1]). In the crystal, ox-MJ0499 forms a dimer structure which is formed with a monomer at the crystallographic position of *I*222 ($-x-1$, y, $-z$). Its interface area was 1285.8 Å^2, which corresponds to 7.5% of the monomer surface (Fig. 1*b*), and eight hydrogen bonds contribute to dimer formation from the *PISA* result (Krissinel & Henrick, 2007). The α3 helix and the following α3–β3 loop of domain 1 interact with the α16 helix and the α16–β16 loop of domain 3 from the other monomer.

[1] Supporting information has been deposited in the IUCr electronic archive (Reference: XB5075).

3.2. Overall structure of MJ1003

The asymmetric unit of MJ1003, consisting of two molecules, was determined at 2.5 Å resolution by molecular replacement using the ox-MJ0499 structure. The monomer consisted of 418 residues (residues 1–418) and lacks the C-terminal residues 419–420. The monomer is composed of 16 α-helices and 16 β-strands, which constitute three domains (domain 1, 1–152; domain 2, 153–271; domain 3, 272–420; Fig. 1*c*). The monomer architecture has a layered sandwich structure similar to that of MJ0499 and the three domains are assembled *via* the four cysteine residues involved in Fe–S cluster binding at the centre. The cysteine residues are in the reduced state, but the Fe–S cluster was unbound. The two molecules of MJ1003, *A* and *B*, superpose with a root-mean-

square deviation (r.m.s.d.) of 0.54 Å (Supplementary Fig. S2*a*). The overall structures of the two molecules are identical, except for the α2 and α6 helices, which contribute the molecular contacts in the crystal.

The MJ1003 crystal has two dimeric forms. In the first, two molecules in the asymmetric unit create a dimeric structure (dimer 1) with an interface area of 924.5 Å^2, which corresponds to 5.6% of the monomer surface (16 487.1 Å^2; Supplementary Fig. S2*b*). The second form (dimer 2) is found in the crystal at the crystallographic position of $P2_12_12_1$ ($-x$ + 1/2, $-y$, z − 1/2) (Fig. 1*d*). A tight dimer interaction is observed with an interface area of 1732.2 Å^2, which corresponds to 10.5% of the monomer surface. The *PISA* results (Krissinel & Henrick, 2007) showed that in dimer 1 the α2 and α6 helices from each monomer interact with each other. In dimer 2, the α3 helix and the α3–β3 loop in domain 1 and the α13 and α14 helices and the α14–β13 loop of domain 3 contribute to dimer formation. 13 hydrogen bonds and four salt bridges contribute to the dimer 2 interface. Superposition of this dimeric structure with aconitase reveals that dimer 1 intrudes on the expected binding site of the small subunit, whereas dimer 2 does not. Dimer 2 has two exposed active sites, and its structure is such that it can form a heterotetramer with two small subunits, while the conformation of dimer 1 is not in a suitable orientation for heterotetramer formation. Therefore, we suggest that dimer 2 is more likely to resemble the biologically active configuration and dimer 1 is a crystallographic artifact that originates from the crystal packing. The overall interaction of MJ1003 dimer 2 is greater than that of the MJ0499 dimer (§3.1).

3.3. Structural comparison of aconitase family proteins

The large-subunit structures of the IPM isomerase and homoaconitase, ox-MJ0499 and MJ1003, respectively, were superposed on the swine aconitase structure (PDB entry 5acn; Robbins & Stout, 1989; Fig. 2). The r.m.s.d.s between the three structures were 2.2 Å for 347 C$^\alpha$-atom pairs for ox-MJ0499 and aconitase, 1.8 Å for 341 C$^\alpha$-atom pairs for MJ1003 and aconitase and 1.4 Å for 359 C$^\alpha$-atom pairs for ox-MJ0499 and MJ1003. The overall fold of ox-MJ0499 and MJ1003 is homologous to domains 1–3 of aconitase; however, there are significant structural differences in domains 1 and 3. In domain 1, ox-MJ0499 and MJ1003 have a long loop after the α3 helix, whereas aconitase has a helix inserted in the corresponding region. Domains 1 and 3 make a close contact by a helix insertion in aconitase, but the two domains are distant in ox-MJ0499 and MJ1003. A catalytic His101 residue, which is a critical residue in the dehydration–hydration mechanism with Ser642 located in domain 4 of aconitase (Lauble & Stout, 1995; Lloyd *et al.*, 1999), is located on the loop following the inserted helix in aconitase. The His62 residue of MJ1003 is located in a similar position to His101 of aconitase, while the His66 residue of ox-MJ0499 is located approximately 11 Å distant. In domain 3, there is a long loop containing a CGPC motif in aconitase and MJ1003, whereas ox-MJ0499 has a short α16 helix formed by the ^{365}CSAC^{369} motif in the corresponding loop region. This α16 helix is located at the centre where His101 is located in aconitase and forms two disulfide bonds with two cysteine residues: Cys102 and Cys304. The catalytic histidine is located similarly in aconitase and MJ1003, despite their structural differences, while MJ0499 shows a quite different structure, including the histidine position.

3.4. Active sites of aconitase family proteins

Members of the aconitase family require an Fe–S cluster for enzyme activation. The substrates of aconitase family proteins have a common structure, except for their diversified γ-moieties: citrate for aconitase, 2-isopropylmalate for IPM isomerase and homocitrate for homoaconitase (Jeyakanthan *et al.*, 2010). The small subunit exerts the substrate specificity of the enzyme through the recognition of different γ-moieties, and the large subunit contains the conserved active site for Fe–S cluster binding. The MJ0499 and MJ1003 proteins, which are the large subunits of homoaconitase and IPM isomerase, respectively, were solved without an Fe–S cluster in the active site (Figs. 3*a* and 3*b*). The active site of aconitase is composed of a complex array of residues that form hydrogen-bonding networks with the substrate and the Fe–S cluster (Robbins & Stout, 1989). In multiple sequence alignments, MJ0499 and MJ1003 have active sites that are well conserved with aconitase, except for two residues: Gln72 and Ile425 in aconitase are substituted by His35 and Met369 in MJ0499 and by His32 and Leu366 in MJ1003 (Supplementary Fig. S3). The MJ1003 protein has three residues, Cys302, Cys362 and Cys365, which

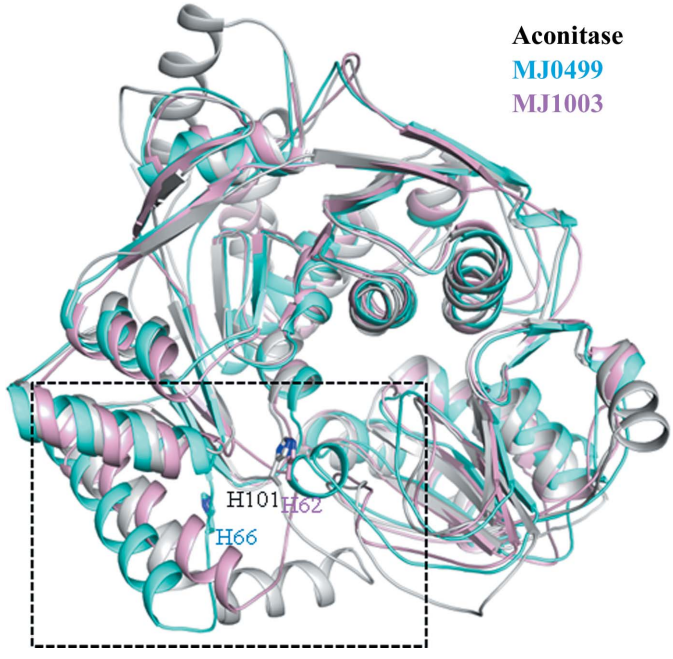

Figure 2
Comparison of aconitase family protein structures. Three protein structures, MJ0499 (cyan), MJ1003 (light pink) and swine aconitase (PDB entry 5acn, grey), are superimposed and the significantly different regions are shown in the box. The catalytic histidine residues, His101 in aconitase, His62 in MJ1003 and His66 in MJ0499, are displayed as stick models.

are conserved ligands of the Fe–S cluster (Fig. 3*a*). Based on its homology to aconitase, Asn209, Leu366 and Asn384 contribute to cluster binding and His32 and Ser118, Arg385 and Arg390 participate in substrate binding. Three conserved ion pairs (Asp61–His62, Asp117–His99 and Glu213–His119) were also observed. Interestingly, the fourth cysteine residue, Cys98, is located at the opposite side to Cys365. In aconitase, it is replaced by Ile146. This residue is located inside the active site, and the S atom of Cys98 is 3.1 Å from Asp61, 5.5 Å from Cys362 and 7.1 Å from Cys302. The active pocket is formed at the centre and is able to bind the incoming Fe–S cluster. The active site of MJ1003 is superposed onto that of aconitase in Fig. 3(*b*). They have similar active-site conformations, including a catalytic histidine residue, His62, in MJ1003 that corresponds to His101 in aconitase (Lauble & Stout, 1995; Lloyd *et al.*, 1999). In aconitase, the Fe–S cluster is bound by three cysteinyl ligands: Cys358, Cys421 and Cys424. MJ1003 and aconitase have structural differences near the Fe–S cluster that include a loop containing Cys365 and Leu366, which is located distantly in the absence of the cluster.

The ox-MJ0499 protein has conserved cysteinyl ligands for the Fe–S cluster, including Cys304, Cys365 and Cys368, and a fourth cysteine residue, Cys102, that is equivalent to Cys98 of MJ1003 (Fig. 3*c*). Two disulfide bonds are formed by the four cysteine residues (Cys102–Cys365 and Cys304–Cys368). The active site of MJ0499 consists of Asn215, Met369 and Asn387 for ligand binding and His35, Ser123, Arg388 and Arg393 for substrate binding. Two conserved ion pairs were identified (Asp122–His103 and Glu219–His124) in MJ0499; however, an ion pair is not formed between Asp65 and His66, which are distant from the active site. There are two salt bridges formed between Arg388 and Asp122 at a distance of 3.0 Å. Near the salt bridges, Met369 (which follows the short helix made by the ^{365}CSAC^{368} motif) is located near domain 1 and makes close contact with His32.

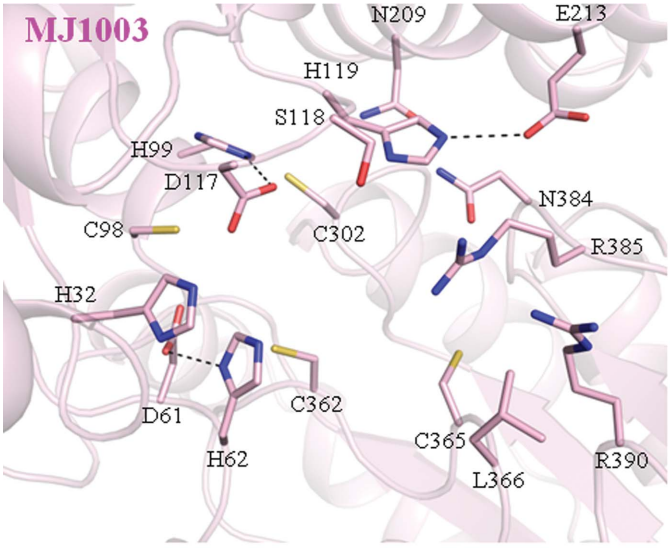

(*a*)

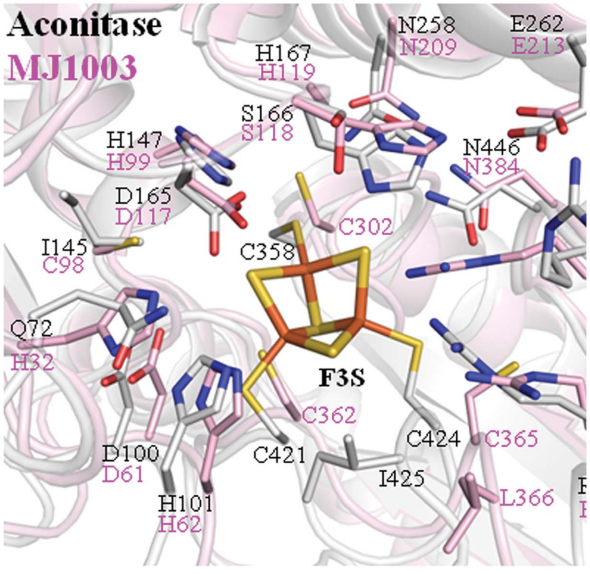

(*b*)

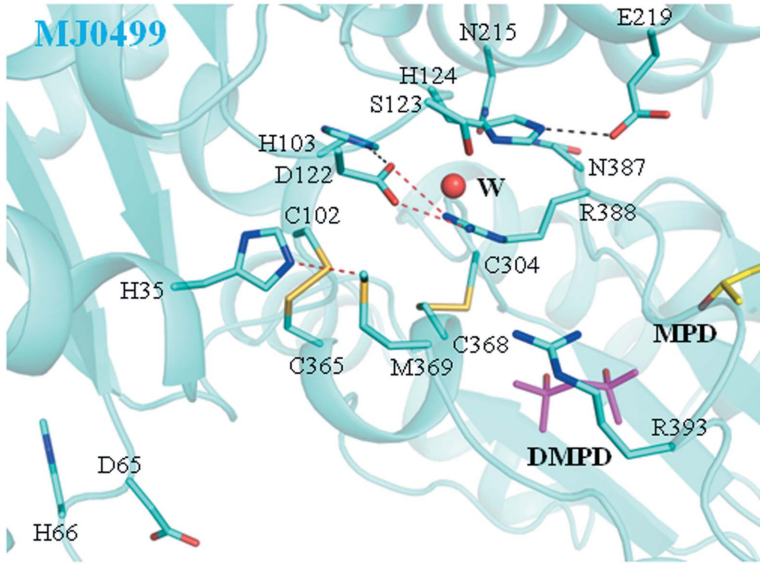

(*c*)

Figure 3
(*a*) Active site of MJ1003. The active-site residues are represented as stick models. No Fe–S cluster is bound at the active site, and four cysteine residues, including the unusual fourth cysteine Cys98, are located at the active site. Three ion pairs, Asp61–His62, Asp117–His99 and Glu213–His119, are indicated by dashed lines. (*b*) Superposition of MJ1003 and aconitase. The structure of MJ1003 (light pink) is superposed onto the Fe–S cluster (F3S)-bound aconitase structure (PDB entry 5acn, grey). The active-site residues of the two proteins are represented as stick models and shown in different colours (black, aconitase; pink, MJ1003). Aconitase binds an Fe–S cluster that is ligated by three cysteine residues. (*c*) Active site of MJ0499. The active-site residues of MJ0499 are represented by a stick model. The well ordered water molecule is shown as a red sphere. MJ0499 lacks the Fe–S cluster and has a fourth cysteine residue, Cys102, at the active site. Two disulfide bonds (Cys102–Cys365 and Cys304–Cys368) are formed. Two ion pairs, Asp103–His122 and Glu219–His124, are indicated by black dashed lines. The specific interactions observed in MJ0499 are indicated by red dashed lines. Arg388 and Asp122 form two salt bridges, and His35 and Met369 come into close contact with each other. The molecules bound near the active site, one molecule each of MPD (yellow) and DMPD (magenta), are displayed as stick models. F3S, [3Fe–4S] cluster; MPD, 2-methylpentane-2,4-diol; DMPD, 2,4-dimethylpentane-2,4-diol.

3.5. Conformational change in red-MJ0499

The disulfide bonds are observed in the active site of ox-MJ0499, which has no space for an incoming Fe–S cluster. To prevent disulfide-bond formation at the active site, red-MJ0499 was prepared with addition of the strong reducing agent TCEP. The crystal structure of red-MJ0499 was solved at 2.6 Å resolution by molecular replacement. The structures of red-MJ0499 and ox-MJ0499 show similar overall folding, and the r.m.s.d. between the two structures was 0.51 Å for 347 C^{α}-atom pairs (Fig. 4*a*). A large conformational change resulting from disulfide-bond dissociation was observed and no bound molecules such as MPD and DMPD were detected in domain 3. The Cys residues Cys102, Csy304, Cys365 and Cys368, which formed disulfide bonds in red-MJ0499, are completely separated (Fig. 4*a*). The ^{365}CSAC^{368} motif is moved outside from the active site and now interacts with the other symmetric molecule (molecule *B*). Two Cys residues, Csy365 and Cys368, are located close to the two symmetrical Cys residues, Cys365′ and Cys368′, from molecule *B* and coordinate a zinc ion at the molecular interface (Supplementary Fig. S4). The Zn^{2+} absorption edge was determined to be 1.28 Å in an X-ray absorption experiment. Interestingly, there is no cavity for

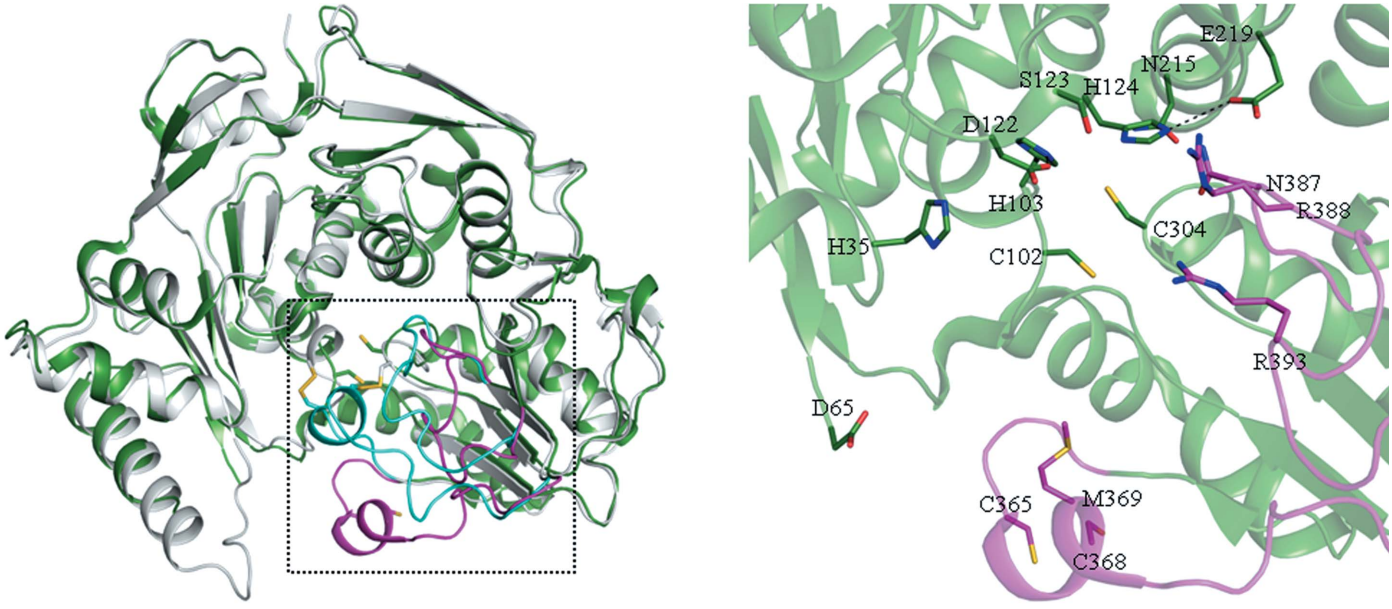

(*a*) (*b*)

Figure 4
(*a*) Overall structure comparison. The two structure forms of MJ0499, ox-MJ0499 (grey) and red-MJ0499 (green), are superimposed. Residues 65–77 are disordered in the red-MJ0499 structure. The square contains the region showing conformational change on the change in redox state between ox-MJ0499 (cyan) and red-MJ0499 (magenta). (*b*) The active site of red-MJ0499. The active-site residues are represented by stick models. The two Cys residues, Cys365 and Cys368, are located distant from the active site.

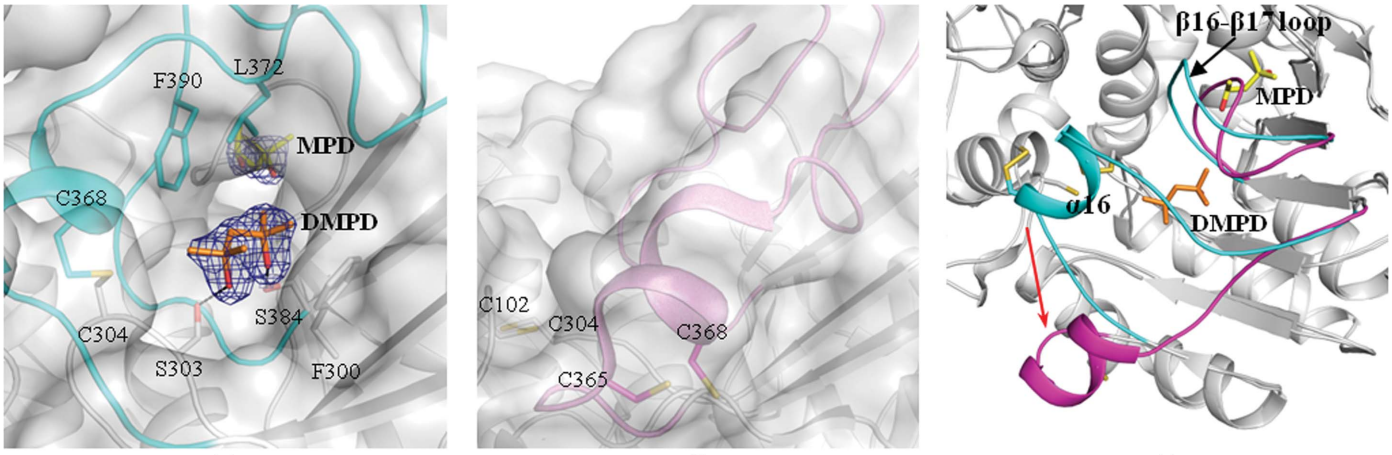

(*a*) (*b*) (*c*)

Figure 5
(*a*) MPD and DMPD binding cavity of MJ0499. A cavity in domain 3 is represented by a surface model. The bound molecules MPD (yellow) and DMPD (orange) and the residues interacting with DMPD are shown as stick models. The electron density for MPD and DMPD is displayed (blue, $2F_o - F_c$ map at 1.5σ cutoff). (*b*) Domain 3 of red-MJ0499 represented in the same view. The cavity is not found in red-MJ0499. (*c*) Domain 3 of ox-M0499 (cyan) and red-MJ0499 (magenta) are superimposed. The α16 helix and the β16–β17 loop show conformational change between the oxidized and reduced states. MPD, 2-methylpentane-2,4-diol; DMPD, 2,4-dimethylpentane-2,4-diol.

MPD molecules following this conformational change. Residues 65–77 in domain 1 are disordered in red-MJ0499. The active-site residues in domains 1 and 2 have similar locations compared with ox-MJ0499, and two ion pairs (Asp122–His103 and Glu219–His124) are also conserved. The residues located in domain 3 (272–420 residues) are placed differently compared with the active site before reduction. Arg388 is located far from Asp122 and they cannot form salt bridges. The red-MJ0499 structure was also compared with the MJ1003 structure, in which all four Cys residues are in the reduced state (Supplementary Fig. S5). The red-MJ0499 β16–β17 loop including Arg388 superposes more closely with MJ1003 than ox-MJ0499, but the ^{365}CSAC^{368} motif is located distant from the ^{362}CGPC^{365} motif of MJ1003.

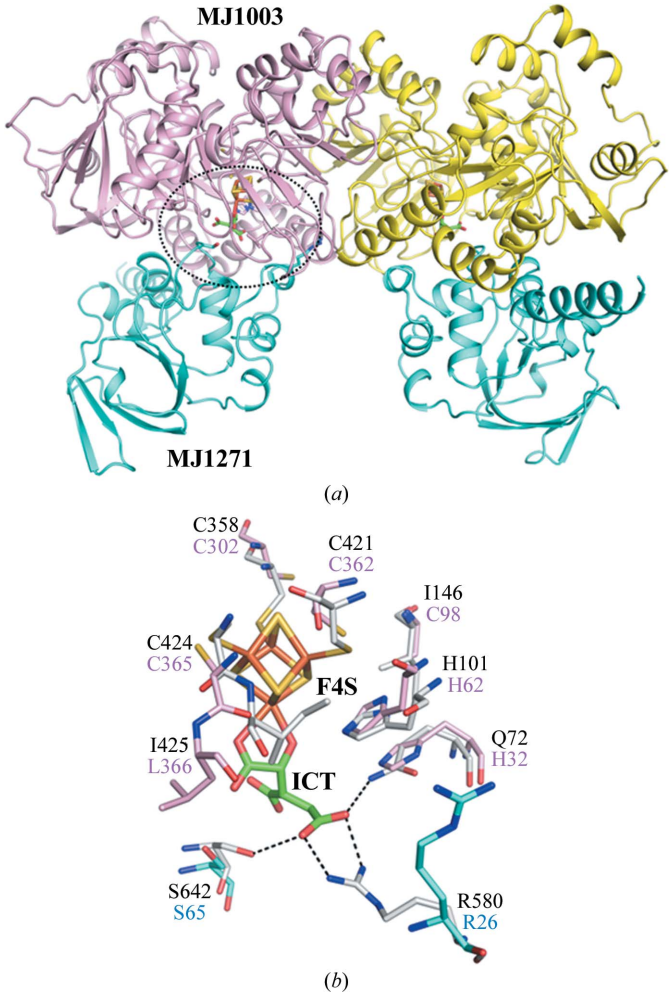

Figure 6
(*a*) Heterotetramer structure of MJ1003. The homoaconitase structure was modelled based on the mitochondrial aconitase structure (PDB entry 7acn; Lauble *et al.*, 1992) using the MJ1003 dimer (light pink and yellow) and two molecules of MJ1271 (PDB entry 2pkp, cyan; Jeyakanthan *et al.*, 2010). The model has two separate active sites at the interface of MJ1003 and MJ1271, which are indicated by dashed circles. The bound molecule of mitochondrial aconitase (green stick model) is displayed with the modelled structure. (*b*) The active-site model of the heterodimer. The active-site residues in MJ1003 (light pink) and MJ1271 (cyan) are shown as a stick representation with the aconitase structure (PDB entry 7acn, grey). Aconitase binds the Fe–S cluster (F4S) and ICT. The interactions between the active-site residues and the γ-moiety of ICT are indicated by dashed lines. F4S, [4Fe–4S] cluster; ICT, isocitrate.

3.6. MPD and DMPD binding in ox-MJ0499

The refined structure of ox-MJ0499 has one MPD molecule and one DMPD molecule bound within the cavity in domain 3 (Fig. 1*a*). The cavity is mainly composed of a parallel β-sheet and several loops. The MPD molecule is bound inside the cavity between the β16–β17 loop (oriented towards the solvent) and the upper β13–β14 loop. This molecule is bound *via* hydrophobic interactions with the surrounding ten residues: Ala277, Pro279-His280-Asn281-Val282, Asn389-Phe390-Arg391, Ile401 and Leu403. The DMPD molecule is bound at the entrance of the cavity surrounded by the long α16–β16 loop, the short α16 helix and the α15–α16 loop. Compared with MPD, this molecule has an additional methyl group at the C4 position. It forms two hydrogen bonds to Ser303 and Ser384 and makes hydrophobic interactions with four residues: Phe300, Cys304, Leu372 and Phe390 (Fig. 5*a*). This cavity in domain 3 is only observed in ox-MJ0499. Domain 3 of ox-MJ0499 was superposed on red-MJ0499, which does not form a cavity (Fig. 5*b*). The β16–β17 loop and the region including the α16–β16 loop, α16 helix and α15–α16 loop show conformational changes following reduction. The α16 helix is moved outwards and cannot help to create the cavity in red-MJ0499.

3.7. Quaternary-structure model of MJ1003

The biological unit of methanogen homoaconitase is a heterotetramer composed of two large subunits and two small subunits (Drevland *et al.*, 2007). According to gel filtration MJ1003 is a homodimer in solution, and this dimer structure is observed in the crystal. The small subunit of methanogen homoaconitase, MJ1271, has already been reported in the PDB (Jeyakanthan *et al.*, 2010) and we have now determined the large-subunit structure. These structures were used to model the heterotetramer based on the aconitase analogue. Firstly, two molecules of aconitase were superposed on the MJ1003 homodimer, and two molecules of MJ1271 were then superimposed onto each domain of aconitase (Fig. 6*a*). The heterotetramer was modelled using the MJ1003 homodimer, and not MJ1271, in which steric hindrance was found between the superimposed molecules. In the model structure, two active sites were located at each MJ1003–MJ1271 heterodimer interface, and the two modelled molecules of MJ1271 did not interact with each other. Therefore, the assembly of heterodimers into heterotetramers is mediated by homodimer interaction of the large subunit, not by the small subunit. The active site formed by the heterodimer interface is shown superposed onto the isocitrate-bound aconitase structure (Fig. 6*b*). Methanogen homoaconitase recognizes (homo)$_{1-3}$-citrate as a substrate, which has a longer 1–3 chain in the γ-moiety than the substrate of aconitase (citrate; Drevland *et al.*, 2007). The substrate specificity is mainly determined by MJ1271, which has Arg26 (in a flexible loop) that functions similarly to Arg580 of aconitase (Jeyakanthan *et al.*, 2010).

The residues of the large subunit make some contribution to substrate recognition. In aconitase, two residues, Gln72 and Ile425, are involved. In the ligand-bound form, Ile425 is located near the γ-moiety and the side chain of Gln72 forms a hydrogen bond to the carboxylate O atom of the γ-moiety. These residues are replaced by Leu366 and His32 in MJ1003, which are more hydrophobic, interacting with the longer carbon backbone of its γ-moiety. In addition, these residues are replaced by Met369 and His35 in MJ0499, which is specific for substrates containing a hydrophobic γ-moiety.

4. Discussion

IPM isomerase and homoaconitase belong to the aconitase family of proteins, which have an Fe–S cluster-binding site composed of three cysteine residues. Three of the Fe centres are coordinated by cysteinyl ligands, and the fourth Fe is a labile ion that binds the substrate (Lloyd *et al.*, 1999; Flint & Allen, 1996). In the active site of MJ1003, a fourth cysteine, Cys98, is located near the three cysteine ligands. Fungal and eubacterial homoaconitases have a conserved glycine residue at the corresponding site (Supplementary Fig. S6*a*). MJ0499 also has a fourth cysteine, Cys102, which forms a disulfide bond to Cys365, one of the three cysteine ligands, whereas a valine is conserved in other IPM isomerases (Supplementary Fig. S6*b*). Only methanogen enzymes have the fourth cysteine at the active site, but its role is not clear. Methanogens are anaerobic organisms and cannot function under aerobic conditions. The fourth cysteine may function as an oxygen sensor through formation of a disulfide bond. Superposition with the aconitase structure showed that the fourth cysteine residue seems to be located near an S atom of the Fe–S cluster, so it might assist in ligand binding at the active site. Further research is required to investigate the functions of this cysteine.

The active-site residues are conserved between MJ0499 and MJ1003, while the residue orientation is quite different. Both proteins were purified under aerobic conditions; however, only ox-MJ0499 forms disulfide bonds. The active site of MJ1003 has three cysteine residues that are easily exposed and accessible to the Fe–S cluster, which is defined as the 'open' state. This region in ox-MJ0499 has two disulfide bonds that are buried inside by other residues: His32, Asp122, Met369 and Arg388. The active pocket is not formed in the active site of ox-MJ0499, which is defined as the 'closed' state. The 'open' active site of MJ1003 is predictable owing to the missing cluster; however, the 'closed' active site of ox-MJ0499 is surprising. The 'open' active site is able to bind the cluster in the active pocket, while the 'closed' active site is not accessible. For enzyme activation, ox-MJ0499 should perform a conformational change from 'closed' to 'open' and then finally the 'activated' state: the cluster-bound structure similar to aconitase (Fig. 7). To test this hypothesis, we have solved the red-MJ0499 structure, which has no disulfide bonds in the active site. The β16–β17 loop containing residues Arg388 and Arg393 has a similar conformation to that in MJ1003, while the ^{365}CSAC^{368} motif of red-MJ0499 extends out from the active site. It shows a new intramolecular interaction with the symmetrical molecule in the dimer (molecule *B*) according to crystal packing. Red-MJ0499 was purified as a monomeric form, although two Cys residues of its CSAC motif interacted with the same motif of the symmetric molecule in the crystal. Overall, the active site of red-MJ0499 would be similar to the active site of MJ1003. The structures of MJ1003 and red-MJ0499 may show the conformational states achieved before incorporation of the Fe–S cluster and combination with the small subunit, which generates the complete activated structure. In addition, this 'closed' state of ox-MJ0499 is only observed in methanogens owing to the fourth cysteine, which is not conserved in the aconitase family.

Ox-MJ0499 has a cavity in domain 3 composed of several loop regions which binds one molecule of MPD and one molecule of DMPD (Fig. 5*a*). These are tightly bound through hydrophobic interactions, and do not interfere with the active site. The cavity is only observed in ox-MJ0499 and is clearly related to disulfide-bond formation. The ^{365}CSAC^{368} motif of domain 3 is moved towards domain 1 by disulfide-bond formation, and the neighbouring loops also show structural changes. These structural changes create the cavity in domain 3 which binds MPD and DMPD. These molecules are similar to allosteric inhibitors, which are located distant from the active site but inhibit enzyme activity. Their binding in domain 3 prevents the conformational change of the active site from

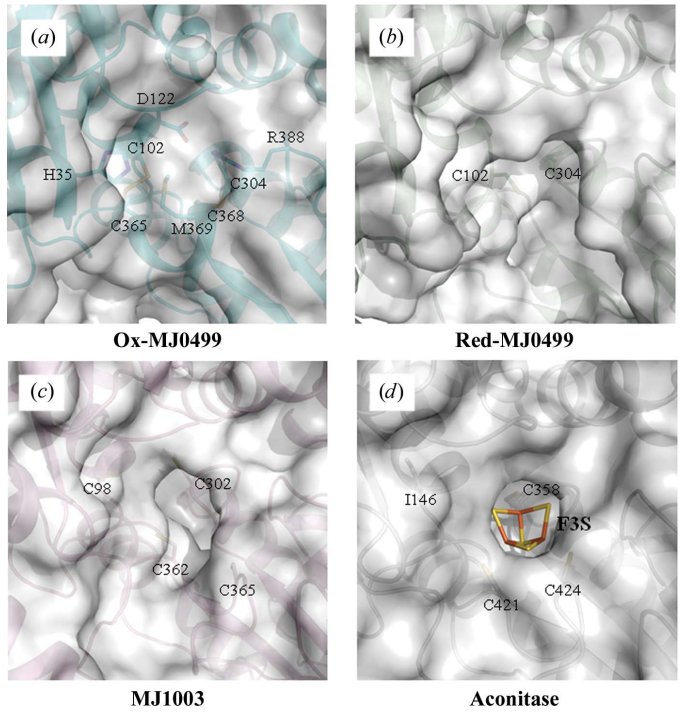

Figure 7
Comparison of the active site in aconitase family proteins. The active sites of four structures, ox-MJ0499, red-MJ0499, MJ1003 and aconitase, are shown as surface models. The active pocket for the Fe–S cluster is observed in MJ1003 but not in ox-MJ0499 and red-MJ0499. (*a*) 'Closed' state of the active site in ox-MJ0499, (*b*) 'widely open' state in red-MJ0499, (*c*) 'open' state in MJ1003 and (*d*) 'activated' state in aconitase (PDB entry 5acn).

the 'closed' state to the 'open' state. This observation will help in the design of new allosteric inhibitors of IPM isomerase.

We thank the staff at the PLS 4A and SPring-8 BL26B2 beamlines for the use of their excellent facilities and assistance with X-ray data collection. We are also grateful to the staff at the Korean Basic Science Institute (KBSI, Daejeon, Republic of Korea) for the use of a Mosquito crystallization robot and the Rigaku MicroMax-007 HF X-ray generator. This work was supported by grants from the National Research Foundation of Korea (2010-0021651).

References

Adams, P. D. *et al.* (2010). *Acta Cryst.* D**66**, 213–221.
Battye, T. G. G., Kontogiannis, L., Johnson, O., Powell, H. R. & Leslie, A. G. W. (2011). *Acta Cryst.* D**67**, 271–281.
Beinert, H. & Kennedy, M. C. (1993). *FASEB J.* **7**, 1442–1449.
Beinert, H., Kennedy, M. C. & Stout, C. D. (1996). *Chem. Rev.* **96**, 2335–2374.
Bult, C. J. *et al.* (1996). *Science*, **273**, 1058–1073.
Chen, V. B., Arendall, W. B., Headd, J. J., Keedy, D. A., Immormino, R. M., Kapral, G. J., Murray, L. W., Richardson, J. S. & Richardson, D. C. (2010). *Acta Cryst.* D**66**, 12–21.
Cole, F. E., Kalyanpur, M. G. & Stevens, C. M. (1973). *Biochemistry*, **12**, 3346–3350.
Drevland, R. M., Jia, Y., Palmer, D. R. & Graham, D. E. (2008). *J. Biol. Chem.* **283**, 28888–28896.
Drevland, R. M., Waheed, A. & Graham, D. E. (2007). *J. Bacteriol.* **189**, 4391–4400.
Emsley, P. & Cowtan, K. (2004). *Acta Cryst.* D**60**, 2126–2132.
Evans, P. (2006). *Acta Cryst.* D**62**, 72–82.
Flint, D. H. & Allen, R. M. (1996). *Chem. Rev.* **96**, 2315–2334.
Fultz, P. N. & Kemper, J. (1981). *J. Bacteriol.* **148**, 210–219.
Gross, S. R., Burns, R. O. & Umbarger, H. E. (1963). *Biochemistry*, **2**, 1046–1052.
Gruer, M. J., Artymiuk, P. J. & Guest, J. R. (1997). *Trends Biochem. Sci.* **22**, 3–6.
Hentze, M. W. & Argos, P. (1991). *Nucleic Acids Res.* **19**, 1739–1740.
Howell, D. M., Harich, K., Xu, H. & White, R. H. (1998). *Biochemistry*, **37**, 10108–10117.
Howell, D. M., Xu, H. & White, R. H. (1999). *J. Bacteriol.* **181**, 331–333.
Jeyakanthan, J., Drevland, R. M., Gayathri, D. R., Velmurugan, D., Shinkai, A., Kuramitsu, S., Yokoyama, S. & Graham, D. E. (2010). *Biochemistry*, **49**, 2687–2696.
Krissinel, E. & Henrick, K. (2007). *J. Mol. Biol.* **372**, 774–797.
Lauble, H., Kennedy, M. C., Beinert, H. & Stout, C. D. (1992). *Biochemistry*, **31**, 2735–2748.
Lauble, H. & Stout, C. D. (1995). *Proteins*, **22**, 1–11.
Lee, E. H., Cho, Y. W. & Hwang, K. Y. (2012). *Biochem. Biophys. Res. Commun.* **419**, 160–164.
Lloyd, S. J., Lauble, H., Prasad, G. S. & Stout, C. D. (1999). *Protein Sci.* **8**, 2655–2662.
Manikandan, K., Geerlof, A., Zozulya, A. V., Svergun, D. I. & Weiss, M. S. (2011). *Proteins*, **79**, 35–49.
Murshudov, G. N., Skubák, P., Lebedev, A. A., Pannu, N. S., Steiner, R. A., Nicholls, R. A., Winn, M. D., Long, F. & Vagin, A. A. (2011). *Acta Cryst.* D**67**, 355–367.
Otwinowski, Z. & Minor, W. (1997). *Methods Enzymol.* **276**, 307–326.
Reeve, J. N. (1992). *Annu. Rev. Microbiol.* **46**, 165–191.
Robbins, A. H. & Stout, C. D. (1989). *Proc. Natl Acad. Sci. USA*, **86**, 3639–3643.
Strassman, M. & Ceci, L. N. (1966). *J. Biol. Chem.* **241**, 5401–5407.
Vonrhein, C., Blanc, E., Roversi, P. & Bricogne, G. (2007). *Methods Mol. Biol.* **364**, 215–230.
White, R. H. (1989). *Biochemistry*, **28**, 9417–9423.
Winn, M. D. *et al.* (2011). *Acta Cryst.* D**67**, 235–242.
Yasutake, Y., Yao, M., Sakai, N., Kirita, T. & Tanaka, I. (2004). *J. Mol. Biol.* **344**, 325–333.